Journal o. and Vibration (1998) **210**(2), 243–254

ON THE NUMERICAL MODELLING OF INTERIOR SOUND FIELDS BY THE MODAL FUNCTION EXPANSION APPROACH

V. Jayachandran, S. M. Hirsch and J. Q. Sun

Department of Mechanical Engineering, University of Delaware Newark, DE 19716, *U.S.A.*

(*Received* 7 *January* 1997, *and in final form* 16 *September* 1997)

Much attention has been paid to sound absorption by active or semi-active means in recent years. Such absorbing treatments are usually applied at the boundaries of the controlled acoustic domain. A study of the impedance at the vibrating boundaries of an actively controlled interior sound field may shed some light on the design of semi-active absorption systems. A popular approach to modelling the interior sound field is to use a Green's function in terms of the acoustic eigenfunctions for the rigid enclosure. It is known that the pressure distribution obtained by this approach is accurate in the interior of the domain, and is inaccurate for modelling impedance on the vibrating boundary. This paper studies this inaccuracy quantitatively and its effect on the optimal control of the interior sound field, and also describes a particular solution approach for determining the interior pressure when a model of the sound field is used.

1. INTRODUCTION

Over the past two decades, significant progress has been made in quieting aircraft and automobile interiors by using advanced control theory with modern sensor and actuator technologies. While active noise cancellation (ANC) and active structural acoustic control (ASAC) are two mainstream technologies [1–22], much attention has also been paid to sound absorption by active or semi-active means [23–29]. Sound absorption occurs when the impedance of an absorbing medium such as an active foam or trim panel matches the impedance of the acoustic medium. Since active noise control systems have been demonstrated to successfully reduce interior noise levels in three-dimensional enclosures, a study of the impedance conditions at the vibrating boundaries of such systems may shed some light on the design of semi-active treatments which may be more cost effective. Also, a study of impedance conditions in the vicinity of the acoustic actuators can help in optimally designing the actuator dynamics. To this end, one needs to quantify the acoustic impedance accurately at the interface of the air and the structure. The problem under investigation in this paper assumes that the enclosed sound field is harmonic, which is generally the case in aircraft and other rotorcraft interiors. Given the acoustic pressure, $p(\mathbf{r})$, and velocity, $\mathbf{u}(\mathbf{r})$, of the air, the specific acoustic impedance, $\mathbf{z}(\mathbf{r})$, at any point is given by

$$\mathbf{z}(\mathbf{r}) = \frac{p(\mathbf{r})}{\mathbf{u}(\mathbf{r})}. \tag{1}$$

In the case of harmonic sound fields, the pressure and velocity are related as

$$\mathbf{u}(\mathbf{r}) = \frac{1}{j\omega\rho} \nabla p(\mathbf{r}) \equiv \{u_x, u_y, u_z\}^T. \tag{2}$$

0022–460X/98/070243 + 12 $25.00/0/sv971328

Hence, the modelling accuracy of the impedance depends on the accuracy of the model which determines the pressure. Because of this, we shall focus our attention on the accuracy of the pressure modelling, although our interest is in the impedance. The pressure field in the enclosure can be obtained by solving the integral equation [26, 30],

$$p(\mathbf{r}) = \int_S \left[p(\mathbf{r}_0) \frac{\partial G(\mathbf{r}|\mathbf{r}_0)}{\partial n} + \frac{\partial p(\mathbf{r}_0)}{\partial n} G(\mathbf{r}|\mathbf{r}_0) \right] \mathrm{d}S + j\omega\rho \int_V q(\mathbf{r}_0) G(\mathbf{r}|\mathbf{r}_0)\, \mathrm{d}V, \tag{3}$$

where $q(\mathbf{r}_0)$ represents the interior source distribution, and $G(\mathbf{r}|\mathbf{r}_0)$ is a Green's function satisfying the inhomogeneous Helmholtz equation,

$$(\nabla^2 + k^2) G(\mathbf{r}|\mathbf{r}_0) = -\delta(\mathbf{r} - \mathbf{r}_0). \tag{4}$$

There are many techniques available for modelling interior sound fields, including modal expansions, method of images, finite element and boundary element methods. The modal expansion method proposes to expand every term in equation (3) in terms of the acoustic mode functions for the rigid enclosure. The Green's function in terms of the modal expansion thus satisfies the rigid wall boundary condition and hence, the normal derivative of the Green's function on the boundary is zero. This leads to an explicit and much simplified equation for the pressure,

$$p(\mathbf{r}) = j\omega\rho \int_S u_n(\mathbf{r}_0) G(\mathbf{r}|\mathbf{r}_0)\, \mathrm{d}S + j\omega\rho \int_V q(\mathbf{r}_0) G(\mathbf{r}|\mathbf{r}_0)\, \mathrm{d}V, \tag{5}$$

where u_n is the velocity normal to S. This approach is often used in the studies of active noise control [2, 3, 26, 31–33]. It is appropriate in this case because active noise control is most effective at low frequencies where the sound field is modal [3, 26]. The solution for the pressure obtained by this method retains the modal behavior of the system and hence provides an intuitive description of the sound field. This technique also lends itself easily to obtaining optimal control solutions which minimize the pressure field in the enclosure.

It is known that since the acoustic modes are for the rigid wall enclosure, the solution for the pressure based on the modal expansion, though accurate in the interior of the domain, does not satisfy the vibrating boundary conditions [3, 26, 30]. Since the rigid wall modes satisfy homogeneous Neumann boundary conditions, the velocity predicted at the boundary is identically zero. This inaccuracy in the velocity field is substantial in the vicinity of the vibrating boundaries. Therefore, this technique is inappropriate for determining impedance conditions at the vibrating boundaries of the enclosure. The objective of this paper is to numerically study these inaccuracies and to describe a particular solution approach which allows one to retain the advantages of the modal solution technique without compromising its accuracy. Furthermore, since many studies of ANC and ASAC have been done by using the Green's function in terms of the rigid wall modes, we also perform a quantitative study of the effect of the aforementioned inaccuracies on the noise control performance.

The remainder of the paper is organized as follows. In section 2, this issue of inaccuracy is examined by considering a simple one-dimensional (1-D) boundary value problem. An exact solution, a modal solution by the Green's function and a modal solution based on the particular solution approach are compared numerically. In section 3, the study is extended to the pressure field in a three-dimensional (3-D) acoustic enclosure. The accuracy of the modal solution by the Green's function approach is studied numerically.

Finally, the effect of the modelling inaccuracy on the optimal control performance of the interior sound is examined.

2. A 1-D EXAMPLE

Consider a 1-D Neumann boundary value problem defined by

$$\frac{\partial^2 u}{\partial x^2} + \kappa^2 u = 0, \qquad \frac{\partial u}{\partial x}(0) = a, \qquad \frac{\partial u}{\partial x}(l) = b. \tag{6}$$

Solving the above problem, we have

$$u_E(x) \equiv u(x) = \frac{a \cos[\kappa(x-l)] - b \cos \kappa x}{\kappa \sin \kappa l}, \tag{7}$$

where the subscript of $u_E(x)$ indicates that the solution is exact. $u_E(x)$ represents the interior solution due to disturbances on the boundaries of the domain. The eigenvalues for equation (6) are given by $\kappa_n = n\pi/l$, and the eigenfunctions are given by $U_n = \cos \kappa_n x$ $(n = 0, 1, \ldots, \infty)$. Consider a Green's function $G(\xi, x)$ satisfying the following equation:

$$G_{\xi\xi} + \kappa^2 G = \delta(\xi - x). \tag{8}$$

When the Green's function is represented in terms of an eigenfunction expansion as

$$G(\xi, x) = \sum_{n=0}^{\infty} g_n \cos \kappa_n \xi,$$

we have $G_\xi(0, x) = G_\xi(l, x) = 0$. It can now be shown that [34, 35]

$$u(x) = aG(0, x) - bG(l, x). \tag{9}$$

Hence the solution for the boundary value problem can be obtained as

$$u_G(x) \equiv u(x) = \sum_{n=0}^{\infty} \frac{\varepsilon_n^2 [a - b(-1)^n]}{(\kappa^2 - \kappa_n^2)} \cos \kappa_n x, \qquad \varepsilon_n = \begin{cases} \sqrt{1/l}, & n = 0, \\ \sqrt{2/l}, & n > 0, \end{cases} \tag{10}$$

where the subscript of $u_G(x)$ indicates that the solution is obtained by using a Green's function in terms of the eigenfunctions U_n. Even though the above solution may converge to the exact solution inside the domain, it can never satisfy the boundary conditions in equation (6).

The above problem may also be solved by homogenizing the boundary conditions in the following manner [34]. Consider a solution $u(x)$ given by

$$u(x) = ax + \left(\frac{b-a}{2l}\right) x^2 + q(x), \tag{11}$$

where $q(x)$ satisfies the following equation and homogeneous boundary conditions:

$$\frac{\partial^2 q}{\partial x^2} + \kappa^2 q = -\left(\frac{b-a}{l}\right) - \kappa^2 \left[ax + \left(\frac{b-a}{2l}\right) x^2 \right],$$

$$\frac{\mathrm{d}q}{\mathrm{d}x}(0) = 0, \qquad \frac{\mathrm{d}q}{\mathrm{d}x}(l) = 0. \tag{12}$$

Note that part of the solution $ax + ((b-a)/2l)x^2$ is constructed so that the inhomogeneous boundary conditions are satisfied. We then expand $q(x)$ as well as the forcing term in equation (12) in terms of the eigenfunctions U_n, and get

$$u_P(x) \equiv u(x) = ax + \left(\frac{b-a}{l}\right)\left(\frac{x^2}{2} - \frac{1}{\kappa^2}\right) + \frac{l}{3}\left(a + \frac{b}{2}\right) + \sum_{n=1}^{\infty} \frac{\epsilon_n^2 \kappa^2[(-1)^n b - a]}{\kappa_n^2(\kappa_n^2 - \kappa^2)} \cos \kappa_n x, \tag{13}$$

where the subscript of $u_P(x)$ indicates that it is via the particular solution approach. Note that the particular solution approach retains the modal information of the system with some corrections for improved solution accuracy at the boundaries.

2.1. NUMERICAL RESULTS AND DISCUSSIONS

Numerical results of these three solutions are now presented and the accuracy of the approximate solutions $u_G(x)$ and $u_P(x)$ is examined.

2.1.1. *Solution accuracy*

To determine the accuracy of the approximate solutions, the exact solution $u_E(x)$ is used. Figure 1 shows the difference between $u_E(x)$ and the approximate solutions $u_G(x)$ and $u_P(x)$ over the domain for $\kappa = 2$. We have set $l = 5$, $a = 0$ and $b = 1$; the exact solution at $x = l$ is $-0{\cdot}77$. It is seen from the figure that for the given number of terms N in the series, $u_G(x)$ has a larger error than $u_P(x)$ in the interior of the domain. On the boundary at $x = l$, $u_G(x)$ has an error of approximately 27% while $u_P(x)$ has an error of 3.3%. Hence, the accuracy of the two solutions is markedly different on the boundary. It can be shown that the mean square values of $u_G(x)$ and $u_P(x)$ over the domain are nearly identical.

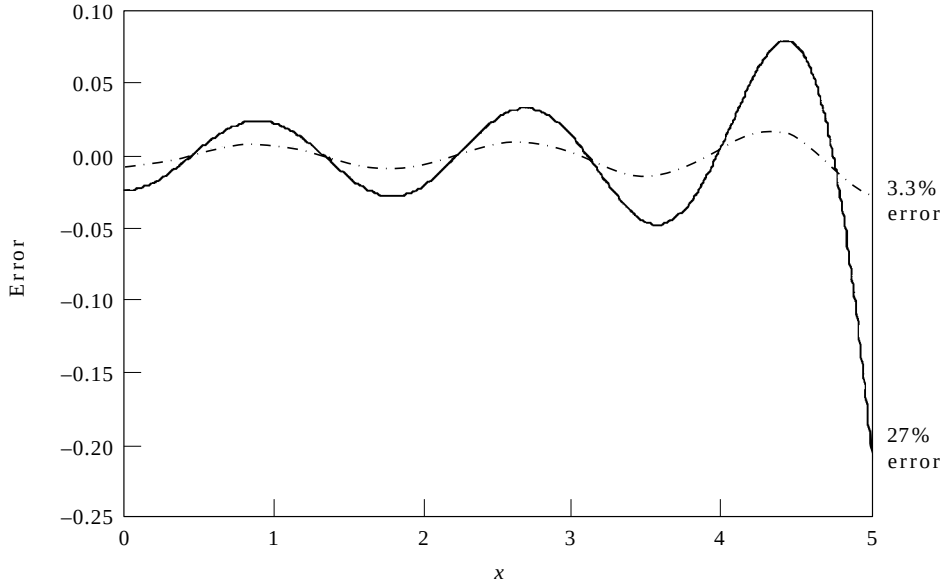

Figure 1. Comparison of error over the domain for $\kappa = 2$. Number of terms in series: $N = 5$.—, $u_G(x) - u_E(x)$; -·-·, $u_P(x) - u_E(x)$.

The percentage error at $x = l$ for an increasing number of terms in the series summation is plotted in Figure 2. The cases when $N = 1$ and 2 have been left out since the number of modes included in the solution is not enough for the given value of κ. As the number of terms increases, the error of $u_P(x)$ quickly converges to zero whereas the error of $u_G(x)$ converges to a finite number, as determined by the Gibbs' phenomenon in the Fourier series [36]. The large error of $u_G(x)$ on the boundaries is mainly due to the fact that $u_G(x)$ is built upon the eigenfunctions which satisfy the homogeneous boundary conditions only. $u_P(x)$, on the other hand, satisfies the inhomogeneous boundary conditions exactly.

2.1.2. *Convergence rate*

The solutions in equations (10) and (13) indicate that the convergence of $u_P(x)$ is faster than $u_G(x)$ by a factor $1/n^2$. Hence, less computational effort is required to compute $u_P(x)$ for the same level of accuracy. It can be shown for the general eigenvalue problem that the convergence rate of $u_P(x)$ is one plus the order of the boundary differential operators higher than that of $u_G(x)$.

3. ACOUSTIC PRESSURE IN A 3-D ENCLOSURE

We now consider the inhomogeneous Helmholtz equation in a 3-D rectangular enclosure with dimensions a, b and c along the x, y and z directions, respectively:

$$(\nabla^2 + \kappa^2)p(\mathbf{r}) = -j\rho\omega q_{vol}(\mathbf{r}). \tag{14}$$

The boundary at $x = a$ vibrates with velocity $w(y, z)$; the remaining boundaries are rigid. The boundary conditions at $y = 0, b$ and $z = 0, c$ are homogeneous

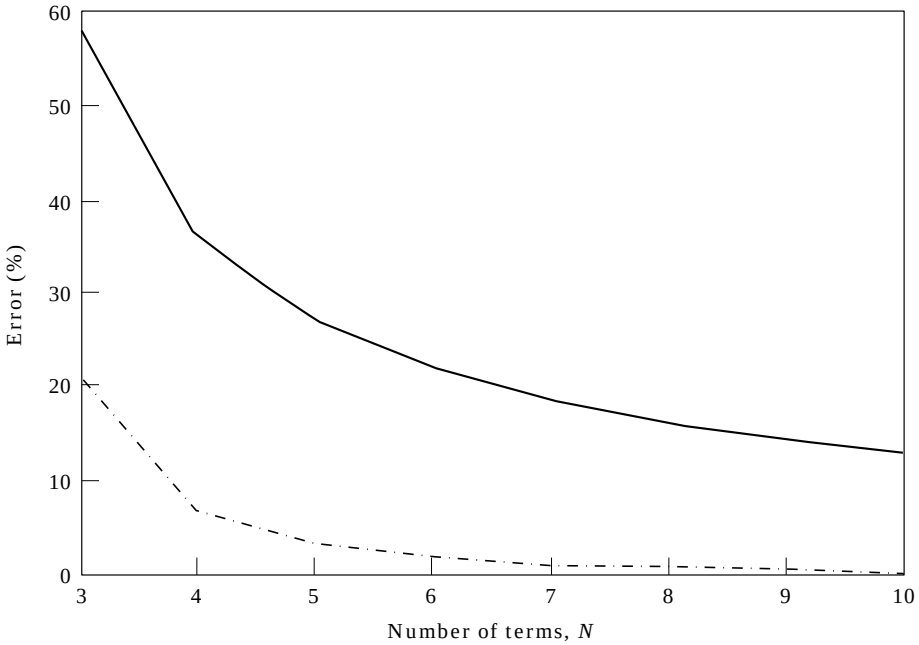

Figure 2. Comparison of percentage errors at $x = l$ for $\kappa = 2$: —, $[u_G(l) - u_E(l)]/u_E(l)$; -·-·-, $[u_P(l) - u_E(l)]/u_E(l)$.

of the Neumann type. In the x direction, they are inhomogeneous and are given by

$$\frac{\partial p}{\partial x}(0) = 0, \qquad \frac{\partial p}{\partial x}(a) = -j\rho\omega w(y, z). \tag{15}$$

The acoustic pressure is given by $p(\mathbf{r}, t) = p(\mathbf{r})\, e^{j\omega t}$, where $\mathbf{r} = \{x, y, z\}$, $\kappa = \omega/c_0$, and c_0 is the speed of sound, ρ is the density of the air and $q_{vol}(\mathbf{r})$ is the interior acoustic source distribution. The eigenvalues and eigenfunctions for the rigid enclosure are the non-trivial solutions of the boundary value problem defined by

$$(\nabla^2 + \kappa^2)\psi(\mathbf{r}) = 0, \qquad \mathbf{r} \in V; \ \nabla\psi(\mathbf{r}) \cdot \mathbf{n} = 0, \qquad \mathbf{r} \in S, \tag{16}$$

where S denotes the boundary of the domain, and $\mathbf{n}$ is the normal of S. The eigenvalues and eigenfunctions are obtained as

$$\kappa_{lmn}^2 = \frac{\omega_{lmn}^2}{c_0^2} = [l\pi/a]^2 + [m\pi/b]^2 + [n\pi/c]^2,$$

$$\psi_{lmn}(\mathbf{r}) = \epsilon_{lmn} \cos(l\pi x/a) \cos(m\pi y/b) \cos(n\pi y/c), \qquad l, m, n = 0, 1, 2, \ldots, \tag{17}$$

where ϵ_{lmn} are the normalization constants.

3.1. SOLUTION TECHNIQUES

Consider only the case when the acoustic medium is excited by the vibration of the surface at $x = a$ and there is no interior source. The solution of the pressure distribution can be expressed in terms of the rigid wall eigenfunctions in the y and z directions,

$$p(\mathbf{r}) = \sum_{m=0}^{\infty} \sum_{n=0}^{\infty} P_{mn}(x) \cos(m\pi y/b) \cos(n\pi z/c), \tag{18}$$

where $P_{mn}(x)$ satisfies the following equation and boundary conditions:

$$\frac{\partial^2 P_{mn}}{\partial x^2} + [\kappa^2 - (m\pi/b)^2 - (n\pi/c)^2]P_{mn} = 0, \qquad \frac{\partial P_{mn}}{\partial x}(0) = 0, \qquad \frac{\partial P_{mn}}{\partial x}(a) = W_{mn}, \tag{19}$$

and

$$-j\rho\omega w(y, z) = \sum_{m=0}^{\infty} \sum_{n=0}^{\infty} W_{mn} \cos(m\pi y/b) \cos(n\pi z/c). \tag{20}$$

Solving the above boundary value problem, we obtain the following solution

$$p_E(\mathbf{r}) = \sum_{m=0}^{\infty} \sum_{n=0}^{\infty} \frac{W_{mn}}{j\alpha} \frac{[e^{j\alpha x} + e^{-j\alpha x}]}{(e^{j\alpha a} - e^{-j\alpha a})} \cos(m\pi y/b) \cos(n\pi z/c), \tag{21}$$

where $\alpha = \sqrt{\kappa^2 - \kappa_{0mn}^2}$. Subscripts of the solutions $p(\mathbf{r})$ hereafter have the same meaning as in section 2. The above solution may be used as the reference solution since it satisfies all boundary conditions.

Following the modal solution approach, we express the Green's function satisfying equation (4) in terms of the eigenfunctions for the rigid enclosure as

$$G(\mathbf{r}|\mathbf{r}_0) = \sum_{l=0}^{\infty} \sum_{m=0}^{\infty} \sum_{n=0}^{\infty} \left[\frac{\psi_{lmn}(\mathbf{r}_0)}{\kappa_{lmn}^2 - \kappa^2} \right] \psi_{lmn}(\mathbf{r}). \tag{22}$$

The pressure distribution in the enclosure without interior sources can be obtained as

$$p_G(\mathbf{r}) = \sum_{l=0}^{\infty}\sum_{m=0}^{\infty}\sum_{n=0}^{\infty} \varepsilon_{lmn}(-1)^l \left[\frac{\psi_{lmn}(\mathbf{r})}{\kappa_{lmn}^2 - \kappa^2}\right] W_{mn}, \tag{23}$$

where the subscript of $p_G(x)$ indicates that the solution is obtained by using the Green's function.

Now, introducing a particular modal solution $P_{mn}(x)$ for equation (18) as

$$P_{mn}(x) = \frac{x^2}{2a} W_{mn} + Q_{mn}(x), \tag{24}$$

where $Q_{mn}(x)$ satisfies homogeneous boundary conditions in the x direction, we can obtain a solution for the pressure by the so-called particular solution approach as

$$p_p(\mathbf{r}) = \sum_{m=0}^{\infty}\sum_{n=0}^{\infty}\left[\frac{x^2}{2a} - \frac{a}{6} + \frac{1}{a(\kappa_{0mn}^2 - \kappa^2)} - \sum_{l=1}^{\infty} \gamma_{lmn}\cos(l\pi x/a)\right] W_{mn}\cos(m\pi y/b)\cos(n\pi z/c), \tag{25}$$

where

$$\gamma_{lmn} = \frac{2a(-1)^l}{l^2\pi^2}\frac{[\kappa^2 - \kappa_{0mn}^2]}{[\kappa^2 - \kappa_{lmn}^2]}, \qquad l \neq 0. \tag{26}$$

Again, similar to the 1-D case, the solution $p_P(x)$ by the particular solution approach satisfies all boundary conditions exactly. It can also be shown that the velocity field predicted by this approach matches that of the vibrating boundary. Hence, this solution can accurately predict the impedance at the boundaries. On the other hand, $p_G(x)$ gives rise to zero velocity at the boundary, and the prediction of the velocity in the vicinity of the vibrating boundary is poor.

3.2. NUMERICAL RESULTS AND DISCUSSIONS

The following ratio of the root mean square (r.m.s.) values of the pressure on different plane sections along the x-axis is used to characterize the error of the solutions by the two above methods:

$$P_G^{err}(x) = \left[\int_0^b\int_0^c |P_G(\mathbf{r}, t) - P_E(\mathbf{r}, t)|^2 \,\mathrm{d}y\,\mathrm{d}z\right]^{\frac{1}{2}} \Big/ \left[\int_0^b\int_0^c |p_E(\mathbf{r}, t)|^2 \,\mathrm{d}y\,\mathrm{d}z\right]^{\frac{1}{2}}. \tag{27}$$

Note that $P_P^{err}(x)$ for $p_P(\mathbf{r})$ is determined by replacing $p_G(\mathbf{r})$ with $p_P(\mathbf{r})$ in equation (27). The numerical results are plotted in Figure 3. Five terms are used in modal summation for each direction, resulting in a total of 125 acoustic modes included in the computation. Recall that the vibrating source is at $x = a$. $p_P(\mathbf{r})$ is seen to perform better than $p_G(\mathbf{r})$ overall, and the error of $p_G(\mathbf{r})$ increases near the vibrating boundary, as expected. The percentage errors of the r.m.s. pressure at the vibrating surface for different frequencies are plotted in Figure 4. It is seen from the figures that on the boundary, $p_P(\mathbf{r})$ is consistently more accurate than $p_G(\mathbf{r})$. Similar to the 1-D case, $p_P(\mathbf{r})$ converges much faster than $p_G(\mathbf{r})$.

From the above discussions, it is evident that the particular solution approach not only satisfies the boundary conditions exactly, but also gives rise to a more accurate solution

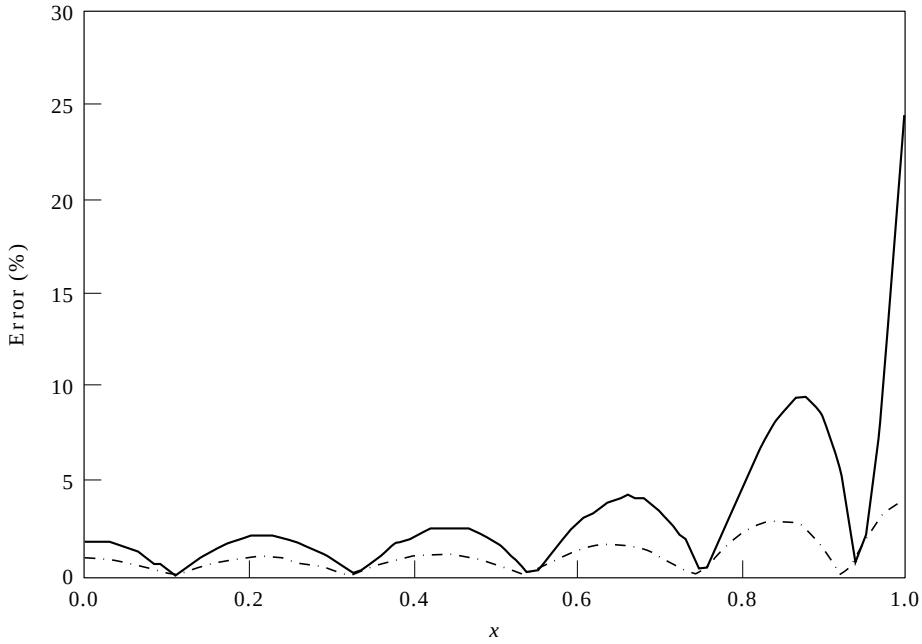

Figure 3. Percentage error of the r.m.s. pressure on the plane sections along the x-axis in the 3-D rectangular enclosure (frequency = 150 Hz): —, $P_G^{err}(x)$; -·-·, $P_F^{err}(x)$.

for the pressure, both in the interior as well as at the boundary of the domain. This approach proves satisfactory for determining the acoustic impedance in the enclosure.

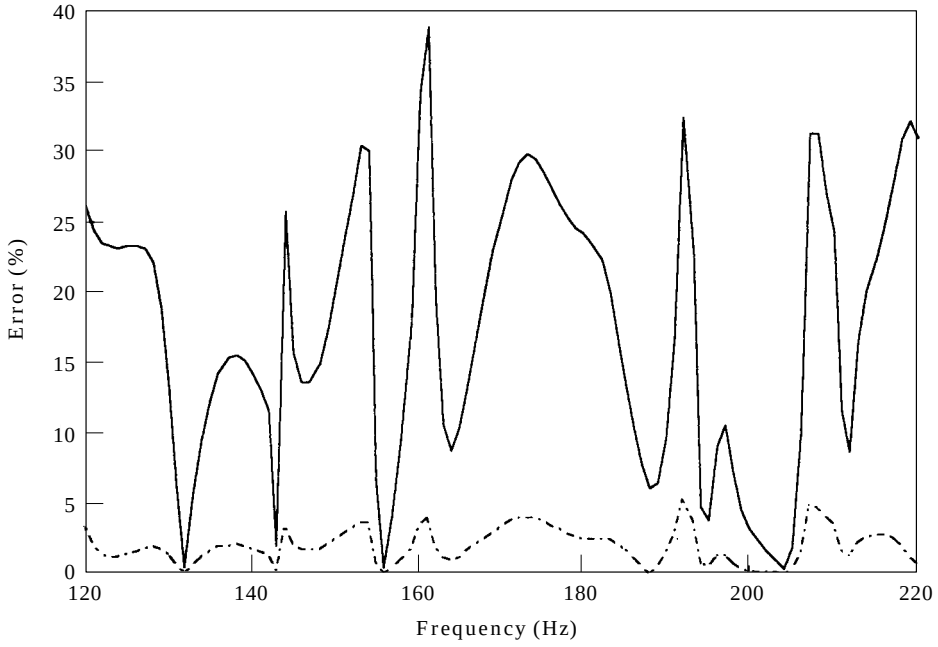

Figure 4. The r.m.s. pressure field error on the vibrating wall ($x = a$): —, $P_G^{err}(l)$; -·-·, $P_F^{err}(l)$.

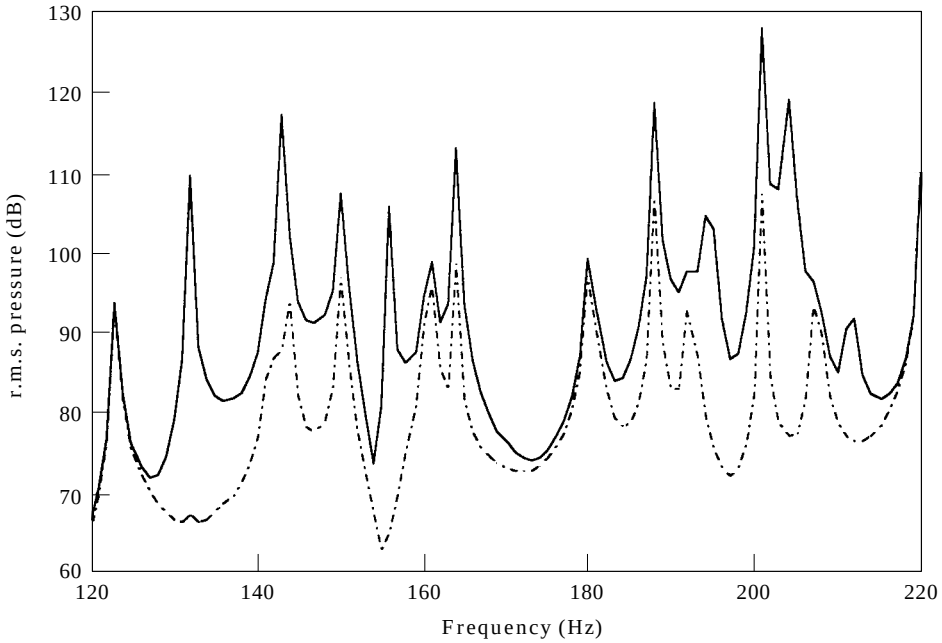

Figure 5. The r.m.s. pressure 20 $\log_{10}$ ($\sqrt{J}/p_o$) in the 3-D enclosure: —, before control; -·-·, after control.

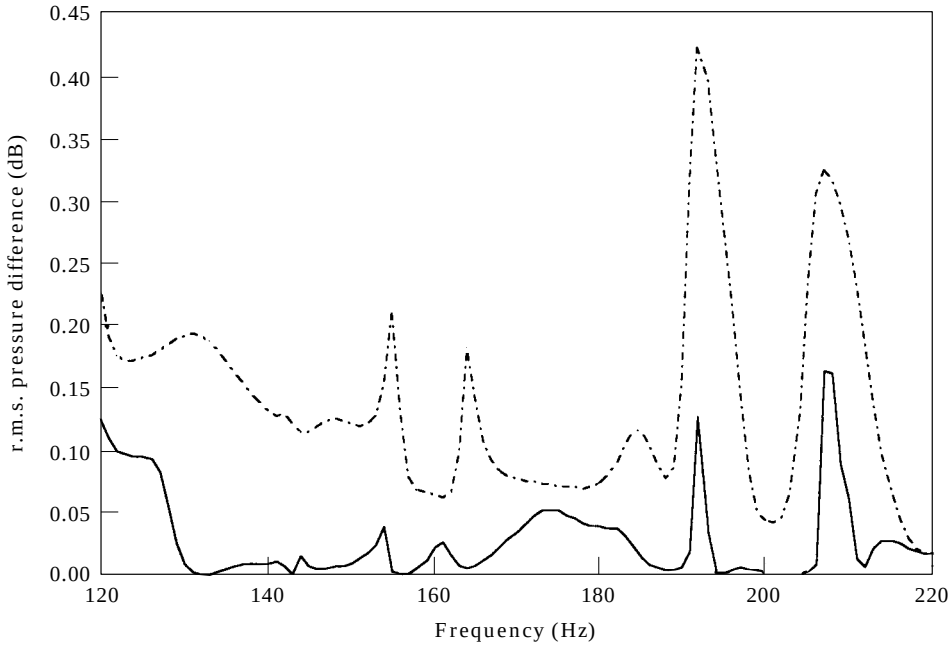

Figure 6. Difference in the performance index based on the two different approximate solutions for the 3-D enclosure: —, before control; -·-·, after control.

3.3. EFFECT ON THE GLOBAL SOUND MEASURE AND OPTIMAL CONTROLS

It can be seen from the previous sections that the modal solution technique using the Green's function is inaccurate on the domain boundaries. It was also observed to have a higher error in the interior of the enclosure than the particular solution approach. Here, a global performance measure based on these two solutions is compared, as well as the resulting optimal controls of the system.

In the 3-D enclosure, the vibrating wall at $x = a$ is taken as the primary sound source and the control sources are modelled as a 2×2 grid of square pistons mounted on the wall at $x = 0$. Assume that the problem is harmonic. The optimal control vector is obtained by minimizing the following cost function [26]:

$$J[\mathbf{u}(y, z), w(y, z)] = \int_V pp^* \, \mathrm{d}x \, \mathrm{d}y \, \mathrm{d}z, \tag{28}$$

where V denotes the volume of the enclosure, p^* is the complex conjugate of p, $\mathbf{u}(y, z)$ is a complex vector representing the vibration amplitude and phase of the control pistons, and $w(y, z)$ is the velocity field of the vibrating wall at $x = a$. The optimal controls are determined using the solutions obtained by both the Green's function method with rigid wall eigenfunctions and the particular solution approach. The r.m.s. pressure before and after control are shown in Figure 5. The optimal controls obtained from the two approximate solutions result in an almost identical optimal performance index. Therefore, only one controlled response is shown. The difference between the optimal performance indices J_{opt} by the two controls is shown in Figure 6 and is less than $\frac{1}{2}$ dB. The percentage difference in the norms of the two control vectors, shown in Figure 7, is very small over a broad frequency range. These results cleraly show that the inaccuracies at the boundary do not affect the control prediction much.

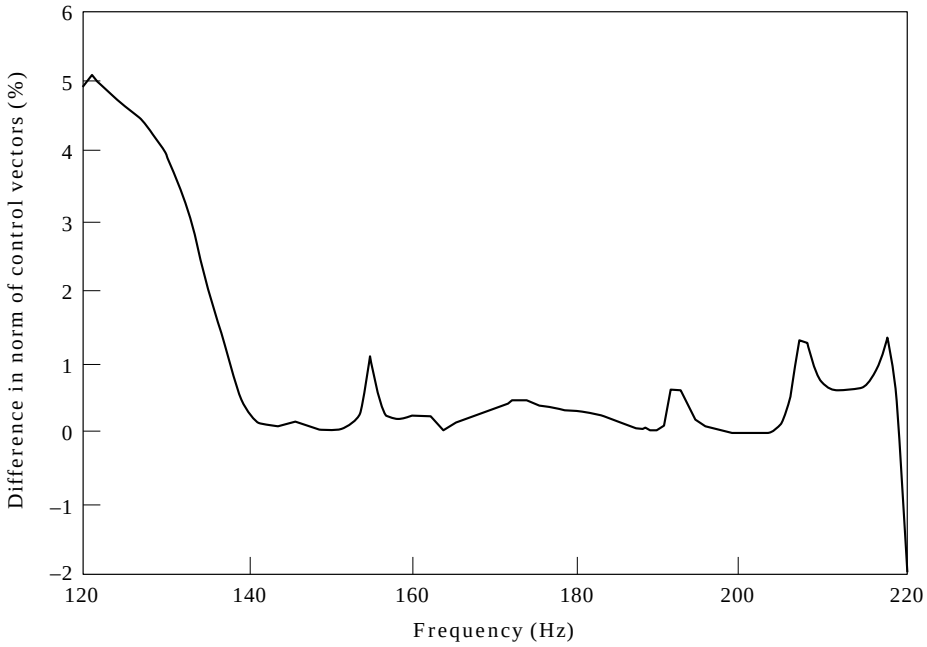

Figure 7. Percentage difference in the norm of the optimal control vectors $(\|u_G\| - \|u_P\|)/\|u_G\|$ for the 3-D enclosure.

4. CONCLUDING REMARKS

The inaccuracy of the modal solution using the Green's function method at the moving boundaries of a 3-D enclosure has been quantitatively studied. The error is related to a well-known Gibbs' phenomenon in the Fourier series at discontinuities. For modelling acoustic impedance at the vibrating boundary, this solution is shown to be inadequate. A particular solution approach that can satisfy the inhomogeneous boundary conditions exactly retains advantages of the modal model without compromising the solution accuracy, and is recommended for this study. Furthermore, it is shown that this solution approach leads to a faster converging solution than the Green's function solution. It has also been observed through simulations that these two solution methods lead to nearly identical optimal controls and global performance indices.

ACKNOWLEDGMENTS

This work was supported in part by a grant (CMS-9634672) from the National Science Foundation, and a grant from the State of Delaware Research Partnership program and Lord Corporation. We would like to acknowledge the support for Vijay Jayachandran by the University of Delaware Competitive Fellowship, and the support for S. M. Hirsch by the Delaware Space Grant College Fellowship Program during the course of this work.

REFERENCES

1. K. K. Ahuja and J. C. Stevens 1990 *Proceedings of the* 13*th AIAA. Aeroacoustics Conference*, *Tallahassee*, FL. Recent advances in active noise control.
2. B. Balachandran, A. Sampath and J. Park 1996 *Smart Materials and Structures* **5**, 89–97. Active control of interior noise in a three-dimensional enclosure.
3. A. J. Bullmore 1987 *PhD Thesis*, *Univeristy of Southampton*. The active minimisation of harmonic enclosed sound fields with particular application to propeller induced cabin noise.
4. A. J. Bullmore, P. A. Nelson and S. J. Elliott 1990 *Journal of Sound and Vibration* **140**, 191–217. Theoretical studies of the active control of propeller-induced cabin noise.
5. S. J. Elliott, A. R. D. Curtis, A. J. Bullmore and P. A. Nelson 1987 *Journal of Sound and Vibration* **117**, 35–58. The active minimization of harmonic enclosed sound fields, Part III: Experimental verification.
6. C. R. Fuller and R. L. Clark 1992 *Proceedings of the* 4*th Aircraft Interior Noise Workshop*, *NASA Langley*, 191–210. Sound transmission reduction with intelligent panel systems.
7. W. G. Halvorsen and U. Emborg 1989 *Proceedings of General Aviation Aircraft Meeting & Exposition*, *Wichita*, *Kanas*. Interior noise control of the Saab 340 aircraft.
8. J. D. Jones and C. R. Fuller 1989 *AIAA Journal* **27**, 845–852. Active control of sound fields in elastic cylinders by multicontrol forces.
9. S. Lefebvre 1991 *MS Thesis*, *Virginia Polytechnic Institute and State University*. Active control of interior noise using piezoelectric actuators in a large-scale composite fuselage model.
10. H. C. Lester and C. R. Fuller 1986 *Proceedings of the* 10*th AIAA Aeroacoustics Conference*, *Seattle*, *WA*, 1374–1380. Active control of propeller-induced noise fields inside a flexible cylinder.
11. D. S. Mandic and J. D. Jones 1989 *Proceedings of the* 12*th AIAA Aeroacoustics Conference*, *San Antonio*, *TX*. Adaptive active control of enclosed sound fields in elastic cylinders via vibrational inputs–noise attenuation research for advanced turboprop aircraft.
12. L. Meirovitch and S. Thangjitham 1990 *Journal of Vibration and Acoustics* **112**, 237–244. Active control of sound radiation pressure.
13. P. A. Nelson, A. R. D. Curtis, S. J. Elliott and A. J. Bullmore 1987 *Journal of Sound and Vibration* **117**, 1–3. The active minimization of harmonic enclosed sound fields, Part I: Theory.
14. D. J. Rossetti 1992 *MS Thesis*, *North Carolina State University*. Interior acoustic response of a uniform cylindrical shell.
15. D. J. Rossetti and M. A. Norris 1994 *Proceedings of* 35*th AIAA/ASME/AHS/ASC Structures*, *Structural Dynamics*, *and Materials Conference*, *AIAA/ASME Adaptive Structures Forum*,

Hilton Head, *SC*. A comparison of actuation and sensing techniques for aircraft cabin noise control.
16. R. J. Silcox, H. C. Lester and S. B. Abler 1989 *Journal of Vibration*, *Stress*, *and Reliability in Design* **111**, 337–342. An evaluation of active noise control in a cylindrical shell.
17. M. A. Simpson, T. M. Luong, C. R. Fuller and J. D. Jones 1989 *Proceedings of the* 12*th AIAA Aeroacoustics Conference*, *San Antonio*, *TX*. Full-scale demonstration tests of cabin noise reduction using vibration control.
18. J. Q. Sun, M. A. Norris, D. J. Rossetti and J. H. Highfill 1996 *Journal of Vibration and Acoustics* **118**, 676–681. Distribution piezoelectric actuators for shell interior noise control.
19. D. R. Thomas, P. A. Nelson, R. J. Pinnington and S. J. Elliott 1995 *Journal of Sound and Vibration* **181**, 515–539. An analytical investigation of the active control of the transmission of sound through plates.
20. J. Tichy 1991 *Journal of Acoustical Society of Japan* (*E*) **12**, 255–262. Current and future issues of active noise control.
21. E. H. Waterman, D. Kaptein and S. L. Sarin 1983 *Proceedings of Business Aircraft Meeting & Exposition*, *Wichita*, *Kansas*. Fokker's activities in cabin noise control for propeller aircraft.
22. A. H. von Flotow 1991 *Proceedings of AHS/RAE International Technical Specialists Meeting on Rotorcraft Acoustics and Rotor Fluid Dynamics*, *Valley Forge*, *PA*. An overview of possible and not-so-possible tasks for active control of sound and vibration.
23. S. Beyene and R. A. Burdisso 1997 *Journal of the Acoustical Society of America* **101**, 1512–1515. A new hybrid passive/active noise absorption system.
24. P. Darlington and M. R. Avis 1996 *Proceedings of Internoise* **96**, 1121–1126. Noise control in resonant soundfields using active absorbers.
25. G. A. Mangiante 1977 *Journal of the Acoustical Society of America* **61**, 1516–1523. Active sound absorption.
26. P. A. Nelson and S. J. Elliott 1992 *Active Control of Sound*. New York: Academic Press.
27. C. J. Radcliffe and S. D. Gogate 1995 *Proceedings of* 1995 *ASME International Mechanical Engineering Congress and Exposition*. An analytical active acoustic sink controller model for wide band noise control applications.
28. Z. Wu, X.-Q, Bao, V. K. Varadan and V. V. Varadan 1993 *Journal of Smart Materials and Structures* **2**, 40–46. Broadband active acoustic absorbing coating with an adaptive digital controller.
29. Z. Wu, V. K. Varadan, V. V. Varadan and K. Y. Lee 1995 *Journal of the Acoustical Society of America* **97**, 1078–1087. Active absorption of acoustic waves using state space model and optimal control theory.
30. F. Fahy 1985 *Sound and Structural Vibration—Radiation*, *Transmission and Response*. New York: Academic Press.
31. F. Asano and D. C. Swanson 1995 *Journal of the Acoustical Society of America* **98**, 2062–2069. Sound equalization in enclosures using modal reconstruction.
32. P. M. Morse and K. U. Ingard 1968 *Theoretical Acoustics*. Princeton, NJ: Princeton University Press.
33. A. Sampath and B. Balachandran 1995 *Proceedings of Aeromechanics Specialist Conference*, *Farfield County*, *CT*. On performance functions and control mechanisms for interior noise control.
34. M. D. Greenberg 1971 *Application of Green's Functions in Science and Engineering*. Englewood Cliffs, NJ: Prentice-Hall.
35. I. Stakgold 1979 *Green's Functions and Boundary Value Problems*. New York: Wiley.
36. P. M. Morse and H. Feshback 1978 *Methods of Theoretical Physics—Part I*. New York: McGraw-Hill.